nature communications

Article

https://doi.org/10.1038/s41467-025-59421-x

PWWP3A disrupts the assembly of VISA/MAVS signalosome to inhibit innate immune response against RNA viruses

Received: 22 January 2024

Accepted: 22 April 2025

Published online: 01 May 2025

Check for updates

Mengling Shi[1,8], Cong Wang[1,8], Zhen Chen[1,8], Yidan Zhou[2], Liang Yue[3,4], Yu Liu[1], Tiannan Guo[3,4], Jun Shang[5], Haotian Xu[1], Yu Zhang[6], Mengcheng Luo[7] ✉ & Caoqi Lei[1,6] ✉

VISA/MAVS is crucial in antiviral innate immunity. Upon RNA virus infection, VISA recruits TBK1 via TRAFs to mitochondria, inducing IRF3 phosphorylation and type I interferons. However, TBK1 recruitment mechanisms via individual TRAFs are unclear. Here, we reveal that PWWP domain-containing 3A (PWWP3A) serves as a negative regulator of RNA virus-triggered signaling. During viral infection, PWWP3A translocates from nucleus to the mitochondria, competing with TRAF6 for binding to VISA, thereby impeding the recruitment of TBK1 and inhibiting IRF3 activation. However, the extent of PWWP3A-mediated inhibition is regulated by the E3 ligase PJA2, which induces PWWP3A degradation post-infection, highlighting the intricate regulatory network in antiviral immunity. Consistently, PWWP3A deficiency enhances antiviral responses, and *Pwwp3a*$^{-/-}$ mice exhibit elevated levels of type I interferons and displayed greater resistance following RNA virus infection. Together, our findings unveil the inhibitory role of PWWP3A in virus-triggered signaling, which provides insights into preventing excessive immune responses.

The innate immune system is an evolutionarily conserved system that detects and defends against microbial infections, including viruses, bacteria, and parasites. Pathogen-associated molecular patterns (PAMPs) such as viral double-stranded RNA (dsRNA) or dsDNA, are recognized by germline-encoded pattern recognition receptors (PRRs), which include cytosolic dsRNA sensor retinoic-acid-inducible gene-I (RIG-I)-like receptors (RLRs) or dsDNA sensor cyclic GMP-AMP synthase (cGAS). Activation of PRRs initiates a signaling cascade, ultimately inducing the production of type I interferons (IFNs) and proinflammatory cytokines. This rapid response serves to restrict virus infection and subsequently activates the adaptive immune response[1].

The RLR family encompasses RIG-I, MDA5 (melanoma differentiation-associated protein 5), and LGP2 (Laboratory of Genetics and Physiology 2). Each of these RLRs possesses a DEAD/H-box RNA helicase domain capable of recognizing and binding to RNA molecules bearing 5′ triphosphate. While RIG-I and MDA5, but not LGP2, also possess N-terminal tandem CARD domains that are responsible for the recruitment of downstream adaptor protein[2,3]. Upon binding to viral RNA ligands, RIG-I and MDA5 undergo conformational changes and

[1]State Key Laboratory of Virology and Biosafety, College of Life Sciences, Frontier Science Center for Immunology and Metabolism, Wuhan University, Wuhan, China. [2]Department of Epidemiology and Biostatistics, School of Public Health, Wuhan University, Wuhan University, Wuhan, China. [3]Center for Intelligent Proteomics, Westlake Laboratory of Life Sciences and Biomedicine, Hangzhou, China. [4]Key Laboratory of Structural Biology of Zhejiang Province, School of Life Sciences, Westlake University, Hangzhou, China. [5]SpecAlly Life Technology Co. Ltd., Wuhan, China. [6]School of Basic Medical Sciences, Lanzhou University, Lanzhou, China. [7]Hubei Provincial Key Laboratory of Developmentally Originated Disease, TaiKang Center for Life and Medical Sciences, School of Basic Medical Sciences, Wuhan University, Wuhan, China. [8]These authors contributed equally: Mengling Shi, Cong Wang, Zhen Chen. ✉e-mail: luomengcheng@whu.edu.cn; caoqilei@whu.edu.cn

translocate to the mitochondria, where they interact with virus-induced signaling adaptor (VISA, also known as mitochondrial antiviral signaling protein [MAVS])[4,5]. These associations rapidly cause the aggregation of VISA on the mitochondrial surface, forming larger prion-like polymers[6]. The aggregated VISA functions as a scaffold to recruit various tumor necrosis factor receptor-associated factor (TRAF) proteins, including TRAF2, 3, 5, and 6, through the distinct TRAF-binding motif or sites, to activate TBK1[7,8]. In turn, TBK1 phosphorylates VISA at the consensus pLxIS motif, enabling the recruitment of IRF3, which is subsequently phosphorylated by TBK1. Phosphorylated IRF3 dimerizes, translocates to the nucleus, and initiates the transcription of IFNs[9]. Despite the significance of VISA is well-established, the intricate regulatory mechanisms underlying the assembly VISA-associated signalosome remain elusive.

The PWWP domain containing 3A (PWWP3A, also known as MUM1 or EXPAND1) belongs to the PWWP family, which is considered as chromatin methylation reader[10]. PWWP3A is reported as a DNA damage responsive protein recruited to DNA damage sites by tumor protein p53 binding protein 1 (53BP1) to facilitate the chromatin relaxation and DNA repair[11], Recently, we identified that aged *Pwwp3a*$^{-/-}$ male mice exhibit testicular atrophy, which may be due to alterations in the immune microenvironment[12]. However, the localization of PWWP3A beyond nucleus and its involvement in other physiological or pathological processes remain largely unknown.

Here, we show that PWWP3A is also localized on the mitochondria and is a binding partner of VISA, which negatively modulates the VISA-mediated innate immune response. In consistent, PWWP3A deficiency specifically enhanced the innate immune response to RNA viruses, without altering the response to DNA viruses, in both cellular and mouse models. Mechanistically, PWWP3A competes with TRAF6 for binding to VISA, a crucial step for TBK1 recruitment to VISA and subsequent IRF3 phosphorylation by TBK1. Our findings reveal the role of PWWP3A in modulating the assembly of VISA signalosome, thereby specifically regulating the innate immune response to RNA viruses.

Results

Identification of PWWP3A as a down-regulated protein in response to RNA virus infection

To identify potential regulators involved in virus-triggered innate immune response, we employed tandem mass tagging (TMT)-based shotgun proteomic analysis to explore differential protein expression in murine bone marrow-derived macrophages (BMDMs) with or without sendai virus (SeV) infection. This approach enabled the identification and relative quantification of up-regulated and down-regulated proteins through replicate analysis. Kyoto encyclopedia of genes and genomes (KEGG) analysis revealed an elevation in proteins associated with innate immune and inflammatory responses following SeV infection, validating the effectiveness of the experiment (Supplementary Fig. 1a). Notably, we also observed an enrichment of several DNA damage response (DDR) pathways in the down-regulated proteins (Supplementary Fig. 1a, b). As emerging studies has revealed a deep crosstalk between DNA damage response and innate immune response[13–16], we subsequently conducted a second round of screening using CRISPR/Cas9-mediated knockout of candidates involved in DDRs. The results of quantitative reverse transcription PCR (RT-qPCR) assays indicated that knockout of PWWP3A, among the tested candidates, exhibited the greatest potential to augment SeV-induced *Ifnb1* transcription (Supplementary Fig. 1c). Recently, we identified that aged *Pwwp3a*$^{-/-}$ male mice exhibit testicular atrophy, potentially due to alterations in the immune microenvironment[12]. Consequently, we conducted further investigations into the role of PWWP3A in antiviral innate immune response.

Initially, we verified the down-regulation of PWWP3A expression upon viral infection. Results of immunoblot analysis demonstrated a marked reduction in PWWP3A protein level in SeV-infected human THP-1 and HEK293 cells (Fig. 1a). Furthermore, we generated a knock-in mice with a V5-tag at the N-terminus of endogenous PWWP3A due to the lack of a qualified PWWP3A antibody in mice. The immunoblot analysis of the primary mouse embryo fibroblasts (MEFs) derived from the *V5-Pwwp3a* knock-in mice confirmed that PWWP3A was specifically impaired after the infection with RNA viruses, such as SeV or vesicular stomatitis virus (VSV), but not with the DNA virus herpes simplex virus type 1 (HSV-1) (Fig. 1b). Notably, we observed a gradual downregulation of PWWP3A expression during the initial 12 h after viral infection, followed by a restoration of expression at 24 h post-infection (Fig. 1c). However, RT-qPCR analysis suggested that SeV infection did not affect the transcription of *PWWP3A* gene in either THP1 or HEK293 cells (Fig. 1d). Additionally, treatment with cycloheximide (CHX), a commonly used ribosomal inhibitor that abolishes protein synthesis, markedly enhanced SeV-triggered PWWP3A degradation in both the V5-tagged knock-in MEFs and HEK293 cells (Fig. 1e, f). Furthermore, the proteasome inhibitor MG132 reversed the decreased expression of PWWP3A following SeV infection, suggesting that virus triggered the PWWP3A degradation in a proteasome-dependent manner (Fig. 1g). These experiments collectively indicate that RNA virus infection induce the PWWP3A degradation in both human and mouse cells.

The degradation of PWWP3A is mediated by E3 ubiquitin ligase PJA2

We subsequently investigated the underlying mechanisms of PWWP3A degradation after virus infection. Given that proteasome-mediated protein degradation predominantly relies on polyubiquitin modifications[17], we firstly investigated whether PWWP3A undergoes polyubiquitination after viral infection. Consistently, PWWP3A was polyubiquitinated following SeV infection (Fig. 1h). Secondly, we transfected HEK293 cells with empty vector or Myc-tagged PWWP3A expression plasmids, and performed the affinity purification-mass spectrometry (AP-MS) by using the Myc-antibody, to identify the potential E3 ubiquitin ligase involved in PWWP3A degradation. As shown in Fig. 1i, several E3 ubiquitin ligases were found to associate with PWWP3A. Thirdly, we determined the effects of these potential candidates and found that overexpression of PJA2 significantly inhibited PWWP3A expression (Supplementary Fig. 2a), whereas knockout of PJA2 had the opposite effect (Fig. 1j). Further co-IP assays confirmed the interaction between PJA2 and PWWP3A in overexpression systems (Fig. 1k). Endogenous co-IP experiments demonstrated that PJA2 did not interact with PWWP3A in the resting cells. Following SeV infection, the interaction between PWWP3A and PJA2 became detectable at 6 h, peaked at 12 h, and then decreased (Fig. 1l). In addition, overexpression of PJA2 augmented the K48-linked polyubiquitination of PWWP3A (Fig. 1m), while knockout of PJA2 resulted in the impairment of SeV-induced PWWP3A polyubiquitination (Fig. 1n). In line with these observations, PJA2 deficiency inhibited SeV-induced transcription of downstream genes following SeV infection (Supplementary Fig. 2b). In summary, our findings identify PJA2 as a crucial mediator in the polyubiquitination and subsequent degradation of PWWP3A upon viral infection.

Overexpression of PWWP3A inhibits RNA virus-triggered signaling

As PWWP3A expression was downregulated in response to RNA viral infection, we subsequently examined whether PWWP3A regulates RNA virus-triggered innate immune responses. As shown in Fig. 2a, overexpression of PWWP3A significantly inhibited SeV-triggered activation of IFN-β promoter and ISRE reporter in a dose-dependent manner. While the PWWP3A overexpression did not inhibit IFN-γ-induced activation of IRF1 promoter (Fig. 2b), suggesting that PWWP3A specifically attenuates virus-triggered signaling. RT-qPCR analysis indicated that the overexpression of PWWP3A significantly inhibited SeV-triggered

https://doi.org/10.1038/s41467-025-59421-x

transcription of downstream effector genes, such as *IFNB1*, *ISG56*, and *RANTES* (Fig. 2c). Consistent with these findings, overexpression of PWWP3A substantially impaired the phosphorylation of IRF3 induced by SeV, which is a prerequisite for type I IFNs induction (Fig. 2d). Notably, PWWP3A overexpression did not affect SeV-induced phosphorylation of TBK1, the key kinase response for IRF3 phosphorylation (Fig. 2d). These experiments revealed that PWWP3A inhibits the activation of IRF3 but not TBK1 following virus infection.

Attenuated innate immune response will result in the enhanced virus replication. To assess whether PWWP3A regulated cellular

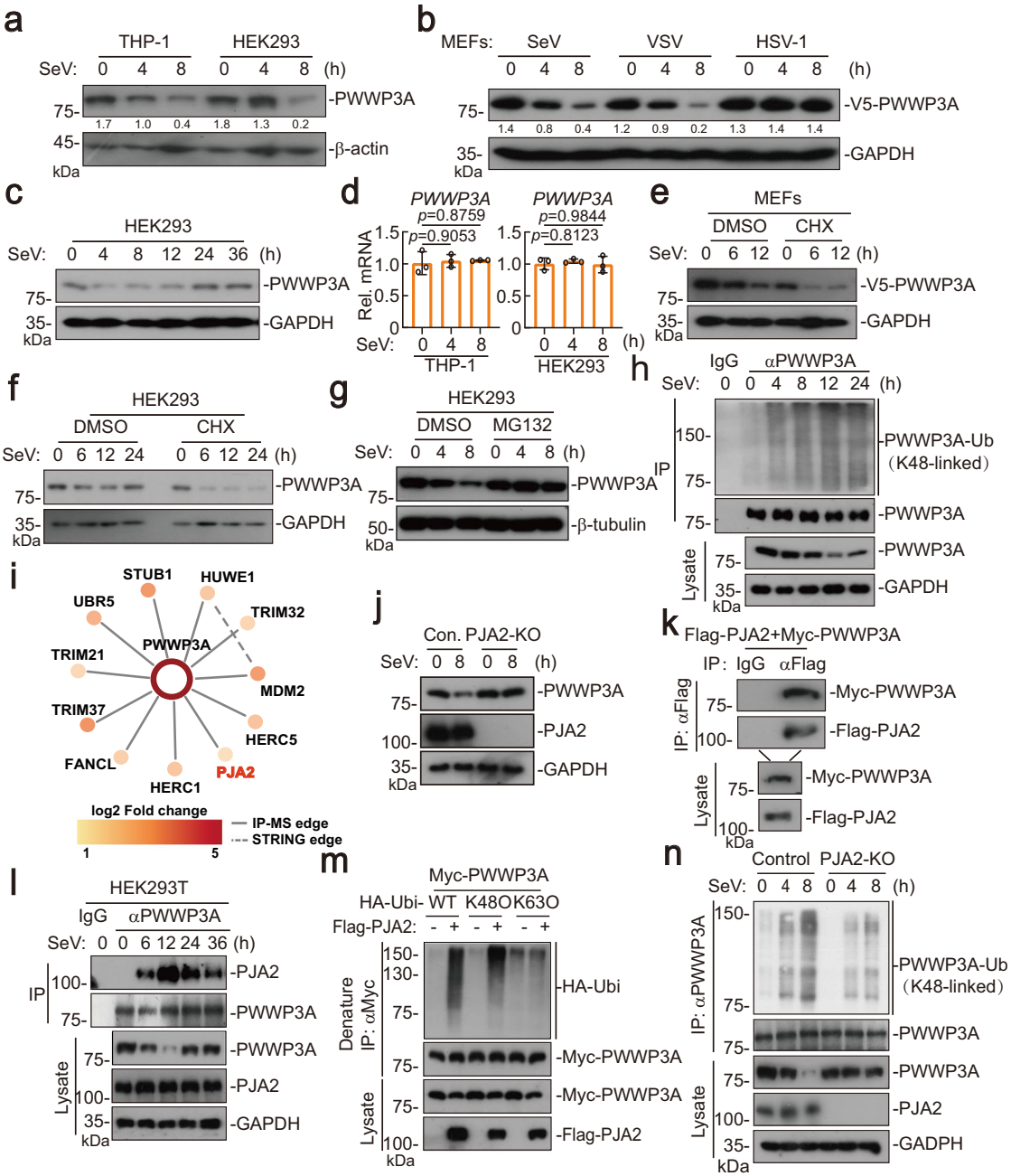

Fig. 1 | PWWP3A undergoes polyubiquitination and degradation in response to RNA virus infection. The human THP-1 and HEK293 cells (**a**), as well as primary *V5-Pwwp3a* knock-in MEFs (**b**) were infected with sendai virus (SeV) (**a, b, c**), vesicular stomatitis virus (VSV) and herpes simplex virus type 1(HSV-1) (**b**) at the indicated time points for the immunoblotting analysis. **d** RT-qPCR analysis of *PWWP3A* (orange) in human THP-1 and HEK293 cells ($n = 3$ biological replicates per group). Primary *V5-Pwwp3a* knock-in MEFs (**e**) or HEK293 cells (**f**) were infected with SeV at the indicated time points, with or without cycloheximide (CHX) treatment (50 μM) for the immunoblotting analysis. **g** HEK293 cells infected with SeV at the indicated time points, with or without MG132 treatment (25 μM) for the immunoblotting analysis. **h** HEK293 cells were infected with SeV at the indicated time points for the co-immunoprecipitation (Co-IP) and immunoblot analysis. PWWP3A-Ubi (K48-linked), the lysine 48-linked ubiquitination chains enriched in PWWP3A proteins. **i** Protein-protein interaction (PPI) map for PWWP3A and E3 ubiquitin ligases. **j** The control (con.) and PJA2-knockout (KO) HEK293 cells were uninfected or infected with SeV for 8 h for the immunoblotting analysis. HEK293 cells were transfected with the indicated plasmids (**k**) or infected with SeV at the indicated time points (**l**) for the co-IP assays and immunoblotting analysis. **m** HEK293 cells were transfected with the indicated plasmids for the denature-immunoprecipitation (Denature-IP) assays. K48O/K63O, all the lysine residues in ubiquitin were mutated to arginine except K48 (K48O) or K63 (K63O). **n** The control and PJA2-KO HEK293 cells were infected with SeV at the indicated time point for the Co-IP assays and immunoblotting analysis. Graphs show mean ± SD, *p* values are from one-way ANOVA (**d**). At least three independent experiments were performed with similar results. Source data are provided as a Source Data file.

https://doi.org/10.1038/s41467-025-59421-x

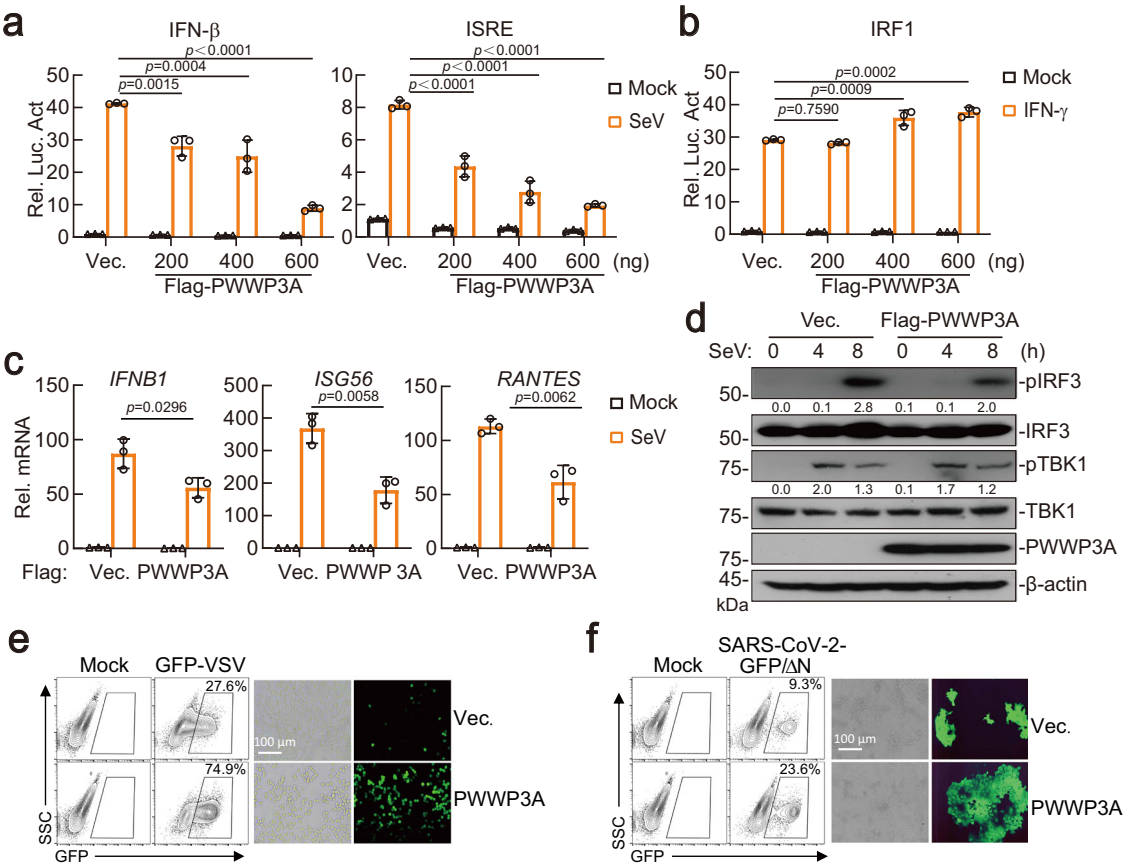

Fig. 2 | Overexpression of PWWP3A inhibits SeV-triggered signaling. HEK293 cells transfected with the interferon-β (IFN-β), interferon stimulated response element (ISRE) (**a**) and Interferon regulatory factor 1 (IRF1) (**b**) reporter and Flag-PWWP3A plasmids for 20 h, then left untreated (blank) or stimulated with sendai virus (SeV, orange) for 10 h (**a**) or interferon-γ (IFN-γ, orange) for 6 h (**b**) before luciferase assays ($n = 3$ biological replicates per group). **c** HEK293 cells were transfected with control or Flag-PWWP3A expression plasmids for 20 h, then the cells were left untreated (blank) or infected with SeV for 8 h (orange) before RT-qPCR analysis ($n = 3$ biological replicates per group). **d** HEK293 cells were transfected with control or Flag-PWWP3A expression plasmids for 20 h, then the cells were infected with SeV at the indicated time points before immunoblotting analysis with the indicated antibodies. The levels of pIRF3 and pTBK1 were quantified using the Chemiluminescence-Imaging program and normalized to the levels of IRF3 and TBK1, respectively. Flow cytometric analysis (left) and fluorescent microscopy analysis (right) of the replication of GFP-VSV in HEK293 cells (**e**) or SARS-CoV-2 GFP/ΔN in Caco2-N cells (**f**). The indicated cells were transfected with control or PWWP3A expression plasmids for 20 h, followed by the infection of GFP-VSV (MOI = 0.1) for 24 h (**e**) or SARS-CoV-2 GFP/ΔN (MOI = 0.1) for 72 h (**f**). Graphs shown as mean ± SD, *p* values are from one-way ANOVA (**a, b**) or two-tailed, unpaired *t*-test (**c**). At least three independent experiments were performed with similar results. Source data are provided as a Source Data file.

antiviral response during RNA viral infection, we infected the control or PWWP3A-overexpressed cells with GFP-tagged VSV and detected the VSV replication by monitoring the GFP expression, and the results suggested that overexpression of PWWP3A potentiated the replication of GFP-tagged VSV (Fig. 2e). Furthermore, we examined the functional contribution of PWWP3A in the defense against SARS-CoV-2. To accomplish this, we employed a well-established system involving the transcription and replication-competent SARS-CoV-2 virus-like-particles (trVLP). In this system, the viral N gene, which is essential for the genome packaging and virion assembly of SARS-CoV2, is substituted by a GFP reporter gene (SARS-CoV-2 GFP/ΔN trVLPs). As a result, the complete viral life cycle can be rescued in the Caco2 cells expressing the SARS-CoV-2 N protein[18]. Using this system, we discovered that overexpression of PWWP3A potentiated SARS-CoV-2 replication in Caco2 cells (Fig. 2f). Taken together, these results highlight the pivotal role of PWWP3A as a negative regulator of virus-triggered signaling.

PWWP3A deficiency potentiates RNA virus-triggered innate immune signaling in human cell lines

To gain a deepen insight into the function of endogenous PWWP3A in antiviral innate immune response, we utilized the CRISPR-Cas9 strategy to generate two PWWP3A-deficient (PWWP3A-KO) HEK293 cell lines (Fig. 3a). RT-qPCR analysis indicated that PWWP3A deficiency significantly potentiated SeV-triggered transcription of downstream effector genes, including *IFNB1*, *ISG56* and *RANTES* (Fig. 3a). Similar results were observed in the human oral epithelial cells (HIOECs) (Supplementary Fig. 3a). Conversely, IFN-γ-induced transcription of *IRF1*, *STAT1* and *GBP2* was comparable between PWWP3A-deficient and control cells (Supplementary Fig. 3b). Consistent with these findings, deficiency of PWWP3A markedly elevated IRF3 phosphorylation induced by SeV (Fig. 3b). Notably, the phosphorylation of TBK1 triggered by SeV was comparable between PWWP3A-deficient and control cells (Fig. 3b). In a similar experiment, deficiency of PWWP3A did not affect IFN-γ-induced phosphorylation of STAT1 (Supplementary Fig. 3c). Furthermore, PWWP3A deficiency resulted in a substantial increase in IRF3 nuclear translocation following SeV infection (Fig. 3c). Consistently, the absence of PWWP3A significantly impaired the replication of GFP-tagged VSV or SARS-CoV-2 (Supplementary Fig. 3d, e). In conclusion, our findings reveal that the absence of PWWP3A augments the innate immune response to RNA viruses in human cell lines.

https://doi.org/10.1038/s41467-025-59421-x

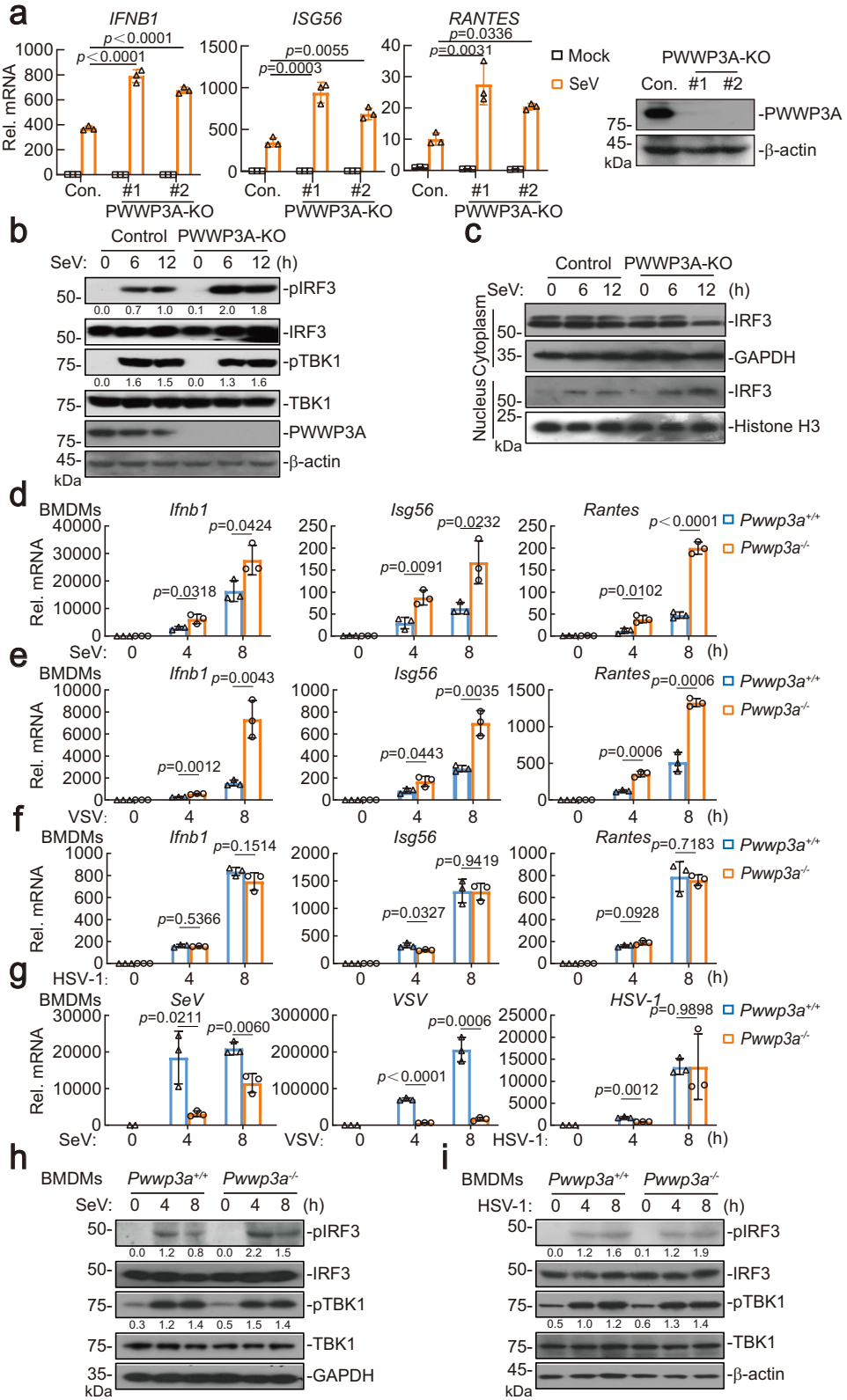

PWWP3A deficiency potentiates RNA virus-triggered innate immune signaling in primary mouse cells

To better characterize the functions of PWWP3A in the antiviral innate immune response, we generated *Pwwp3a*$^{-/-}$ mice using a gene targeting strategy in embryonic stem cells as previously described (Supplementary Fig. 4a, b)[12]. RT-qPCR and genotyping analysis confirmed the successful generation of *Pwwp3a*$^{-/-}$ mice (Supplementary Fig. 4c, d). Subsequently, we prepared BMDMs from both *Pwwp3a*$^{+/+}$ and *Pwwp3a*$^{-/-}$ mice, and infected the cells with different types of viruses, such as RNA viruses SeV and VSV or DNA virus HSV-1. RT-qPCR analysis indicated that the transcription of downstream effector genes, such as *Ifnb1*, *Isg56* and *Rantes*, induced by RNA virus SeV or VSV, was significantly increased in *Pwwp3a*$^{-/-}$ BMDMs (Fig. 3d, e). In contrast, the transcription of these downstream effector genes induced by DNA

Fig. 3 | PWWP3A deficiency potentiates RNA virus-triggered signaling. a The control (con.) and PWWP3A-knockout (KO) HEK293 cells were uninfected or infected (blank) with sendai virus (SeV, orange) for 8 h before RT-qPCR analysis ($n = 3$ biological replicates per group). **b** The control and PWWP3A-KO HEK293 cells were infected with SeV at the indicated time, then the indicated total or phosphorylated proteins were detected by immunoblotting analysis with the indicated antibodies. **c** Cell fractionation analysis of the IRF3 nuclear translocation in control and PWWP3A-KO HEK293 cells infected with SeV at the indicated time points. *Pwwp3a*$^{+/+}$ (blue) and *Pwwp3a*$^{-/-}$ (orange) bone marrow-derived macrophages (BMDMs) were infected with SeV (**d, g**), vesicular stomatitis virus (VSV) (**e, g**) or herpes simplex virus type 1(HSV-1) (**f, g**) at the indicated time points before RT-qPCR analysis ($n = 3$ biological replicates per group). *Pwwp3a*$^{+/+}$ and *Pwwp3a*$^{-/-}$ BMDMs were infected with SeV (**h**) or HSV-1 (**i**) at the indicated time points, then the indicated total or phosphorylated proteins were detected by immunoblotting analysis with the indicated antibodies. The levels of pIRF3 and pTBK1 were quantified using the Chemiluminescence-Imaging program and normalized to the levels of IRF3 and TBK1, respectively (**b, h, i**). Graphs shown as mean ± SD, *p* values are from one-way ANOVA (**a**) or two-tailed, unpaired *t*-test (**d**–**g**). At least three independent experiments were performed with similar results. Source data are provided as a Source Data file.

virus HSV-1 remained similar in both *Pwwp3a*$^{+/+}$ and *Pwwp3a*$^{-/-}$ BMDMs (Fig. 3f). Correspondingly, PWWP3A deficiency significantly impaired the replication of SeV and VSV, but not HSV-1, compared to the control BMDMs (Fig. 3g). Furthermore, the absence of PWWP3A facilitated SeV-triggered phosphorylation of IRF3, but not TBK1, compared to the *Pwwp3a*$^{+/+}$ BMDMs (Fig. 3h). In contrast, PWWP3A deficiency had no impact on HSV-1-induced phosphorylation of either IRF3 or TBK1 in BMDMs (Fig. 3i). Poly(I:C), a synthetic analog of viral RNA, is recognized by cytoplasmic RLRs and membrane-localized toll-like receptor 3 (TLR3) in the cytoplasm and cell culture medium, respectively. Notably, PWWP3A deficiency specifically potentiated cytoplasmic transfected poly(I:C)-triggered RLRs-mediated transcription of downstream effector genes (Supplementary Fig. 5a). However, TLR3-mediated downstream gene transcriptions, induced by cell culture supernatant containing poly (I:C), was comparable between *Pwwp3a*$^{+/+}$ and *Pwwp3a*$^{-/-}$ BMDMs (Supplementary Fig. 5b). Given the high homology between PWWP3B (also known as MUM1L1) and PWWP3A, we also assessed whether PWWP3B exhibited similar functions to PWWP3A in virus-triggered signaling. RT-qPCR analysis revealed the comparable induction of downstream effector genes in BMDMs derived from *Pwwp3b*$^{+/+}$ and *Pwwp3b*$^{-/-}$ mice upon infection with either SeV or HSV-1(Supplementary Fig. 5c, d). These results suggested that PWWP3B was not involved in the antiviral signaling pathways.

Additionally, we isolated mouse lung fibroblasts (MLFs) from *Pwwp3a*$^{+/+}$ and *Pwwp3a*$^{-/-}$ mice and challenged them with SeV or HSV-1. In consistent, PWWP3A deficiency significantly increased transcription of downstream antiviral effectors induced by SeV, but not HSV-1 (Supplementary Fig. 5e, f). Furthermore, the deficiency of PWWP3A enhanced the phosphorylation of IRF3, but not TBK1, following SeV infection, while having no effect on the phosphorylation of IRF3 or TBK1 after HSV-1 infection (Supplementary Fig. 5g, h). These findings further validated the specific role of PWWP3A in RLRs-mediated signaling.

Together, our findings indicate that PWWP3A specifically attenuates the RLRs-mediated innate immune response triggered by RNA viruses in mouse primary immune cells and fibroblasts.

Pwwp3a$^{-/-}$ mice exhibit elevated induction of antiviral cytokines and enhanced resistance against RNA viral infection

To gain insights into the role of PWWP3A in host defense against RNA virus infections in vivo, we performed experiments by infecting *Pwwp3a*$^{+/+}$ and *Pwwp3a*$^{-/-}$ mice with VSV and influenza virus A/Puerto Rico/8/1934 (H1N1) (PR8). As illustrated in Fig. 4a, b, *Pwwp3a*$^{-/-}$ mice exhibited greater resistance to lethal VSV or PR8 infections compared to their control littermates. Whereas both *Pwwp3a*$^{+/+}$ and *Pwwp3a*$^{-/-}$ mice displayed similar sensitivities to HSV-1 infection (Fig. 4c). Consistently, the concentrations of serum IFN-β, IL-6, and MCP-1 in *Pwwp3a*$^{-/-}$ mice were increased compared to their wild-type counterparts following VSV or PR8, but not HSV-1 infection (Fig. 4d-f). Furthermore, there was a significant increase in the transcription of *Ifnb1* and *Isg56* in *Pwwp3a*$^{-/-}$ mice, accompanied by a reduction in VSV or PR8 replication in the lungs or brains, compared to *Pwwp3a*$^{+/+}$ mice (Fig. 4g, h). While PWWP3A deficiency had minimal effects on the transcription of *Ifnb1* and *Isg56*, and led to comparable viral replication in the lungs and brains following HSV-1 infection (Fig. 4i). Collectively, our findings indicate that PWWP3A selectively inhibits the innate immune response to RNA viruses, while having no discernible effect on the immune response to DNA viruses in vivo.

PWWP3A regulates antiviral innate immune response at the VISA level

Having established that PWWP3A impairs RNA virus-triggered innate immune response in both in vitro and in vivo models, we then aimed to determine how PWWP3A inhibited RLRs-mediated signaling. Various proteins, such as RIG-I, MDA5, VISA, TBK1, and IRF3, have been implicated in virus-induced IFN-β activation. Reporter assays indicated that overexpression of PWWP3A efficiently inhibited the activation of IFN-β promoter triggered by RIG-I, MDA5, VISA and TBK1, but not IRF3-5D (a constitutively active mutant of IRF3) (Supplementary Fig. 6a). Conversely, deficiency of PWWP3A had the opposite effect (Supplementary Fig. 6b). Transient transfection and co-IP experiments revealed that PWWP3A interacted with VISA and exhibited a weaker association with TBK1, but not interacted with other tested molecules, such as RIG-I, MDA5, cGAS, MITA or IRF3 (Fig. 5a). The in vitro pull-down assays further indicated that *E. coli*-derived PWWP3A directly interacted with VISA, while no interaction was observed with TBK1 or IRF3 (Fig. 5b). Interestingly, endogenous co-IP experiments suggested that PWWP3A constitutively associated with VISA in uninfected cells, and their interaction was slightly enhanced after SeV infection, despite a concurrent gradual decrease in PWWP3A expression (Fig. 5c). These findings collectively indicate that PWWP3A interacts with VISA, thereby inhibiting RLR-triggered signaling at the VISA level.

Furthermore, we identified the domain(s) mediating the interaction between PWWP3A and VISA. Co-IP experiments revealed that only full-length VISA and its mutants harboring the C-terminal transmembrane domain (TM) associated with PWWP3A, indicating the mitochondrial localization of VISA was essential for its ability to associate with PWWP3A (Supplementary Fig. 7a). In contrast, the deletion of PWWP domain (Δ408-505) not only diminished the ability of PWWP3A to interact with VISA (Supplementary Fig. 7b), but also abolished its inhibitory effects on SeV-mediated transcription of downstream genes (Supplementary Fig. 7c), highlighting the critical role of PWWP domain in its inhibitory function in RLRs-triggered signaling.

Given the importance of the TM domain of VISA in its interaction with PWWP3A, we further investigated the localization patterns of these two proteins utilizing the bimolecular fluorescence complementation (BiFC) assays[19]. In these assays, the N-terminal and C-terminal fragments of YFP (NYFP and CYFP) were fused to PWWP3A and VISA, respectively. As shown in Fig. 5d, co-transfection of NYFP-PWWP3A and CYFP-VISA resulted in successfully reconstitution of YFP fluorescence in HEK293 cells, indicating a physical interaction between PWWP3A and VISA, which brings the two YFP fragments into proximity. It is noted that the reconstituted YFP signal merged with TOM20, a mitochondrial outer membrane protein, indicating a potential interaction between PWWP3A and VISA on mitochondria (Fig. 5d). Since PWWP3A was considered as a nuclear protein, we further examined the impact of SeV infection on its subcellular localization[11]. The cell fractionation assays suggested that, under basal conditions,

https://doi.org/10.1038/s41467-025-59421-x

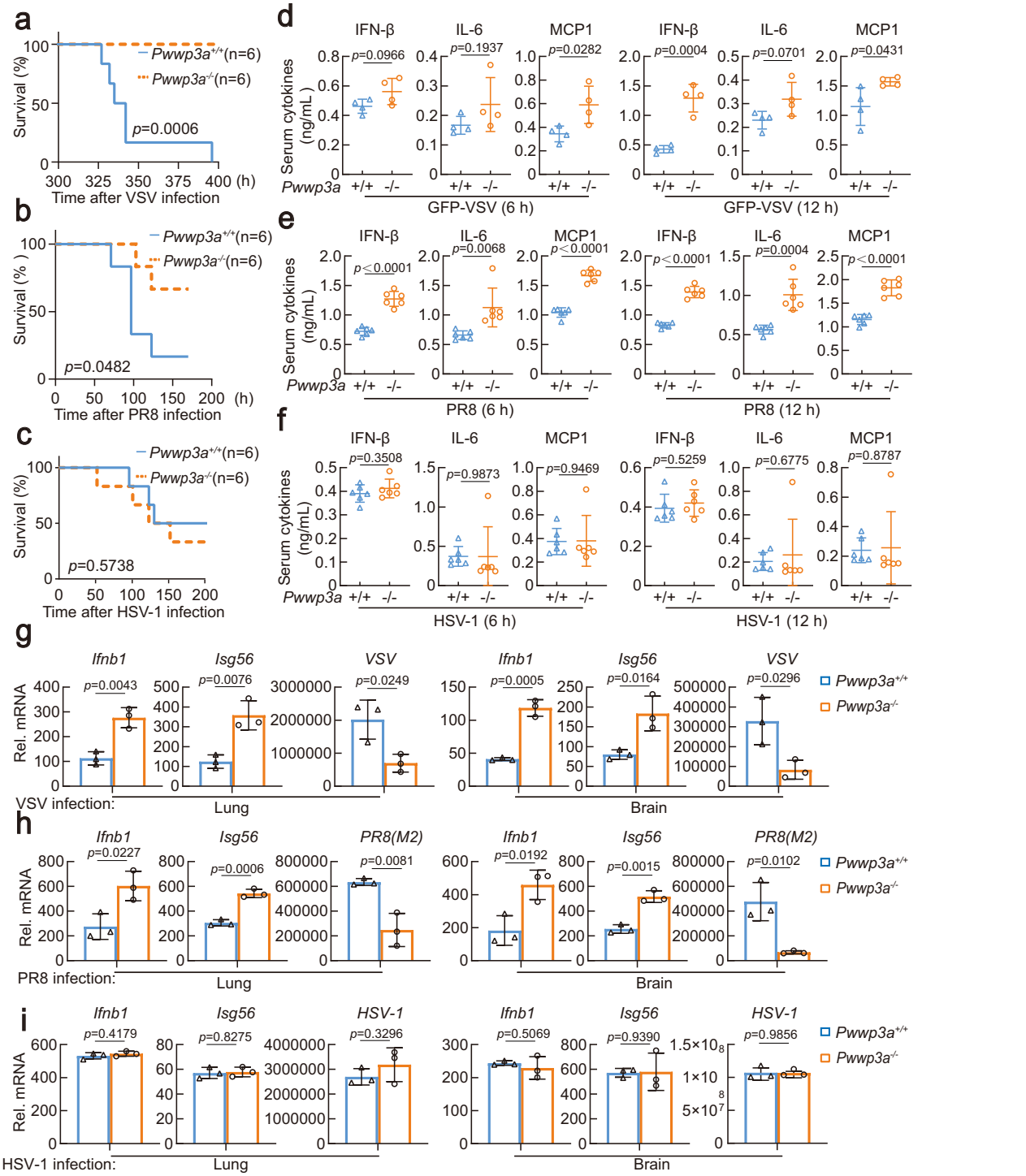

Fig. 4 | *Pwwp3a*$^{-/-}$ mice exhibit elevated induction of antiviral cytokines and enhanced resistance against RNA viral infection. Survival rate of sex- and age-matched *Pwwp3a*$^{+/+}$ (blue) and *Pwwp3a*$^{-/-}$ (orange) mice ($n = 6$) which were intravenously (i.v.) infected with vesicular stomatitis virus (VSV, 2×10^7 PFU per mouse, **a**) or herpes simplex virus type 1(HSV-1, 2×10^7 PFU per mouse, **c**), as well as intranasal inhalation infected with influenza virus A PR8 (10^6 EID50, **b**). The survival of mice was recorded every 12 h. The graphs of survival rate were shown by Kaplan-Meier method and analyzed with log-rank test. The ELISA analysis of the levels of indicated cytokines in sera from *Pwwp3a*$^{+/+}$ (blue) and *Pwwp3a*$^{-/-}$ (orange) mice which were i.v. infected with VSV (2×10^7 PFU per mouse, $n = 4$, **d**) or HSV-1 (2×10^7 PFU per mouse, $n = 6$, **f**), as well as intranasal inhalation infected with influenza virus A PR8 (10^6 EID50, $n = 6$, **e**) at the indicated time points. RT-qPCR analysis of the mRNA abundance of indicated genes in lungs or brains from *Pwwp3a*$^{+/+}$ (blue) and *Pwwp3a*$^{-/-}$ (orange) mice which were i.v. infected with VSV (2×10^7 PFU per mouse, $n = 3$, **g**) or HSV-1 (2×10^7 PFU per mouse, $n = 3$, **i**), as well as intranasal inhalation infected with influenza virus A PR8 (10^6 EID50, $n = 3$, **h**) for 3 days. Graphs shown as mean ± SD, p values are from log-rank analysis (**a**–**c**) or two-tailed, unpaired t-test (**d**–**i**). At least three independent experiments were performed with similar results. Source data are provided as a Source Data file.

https://doi.org/10.1038/s41467-025-59421-x

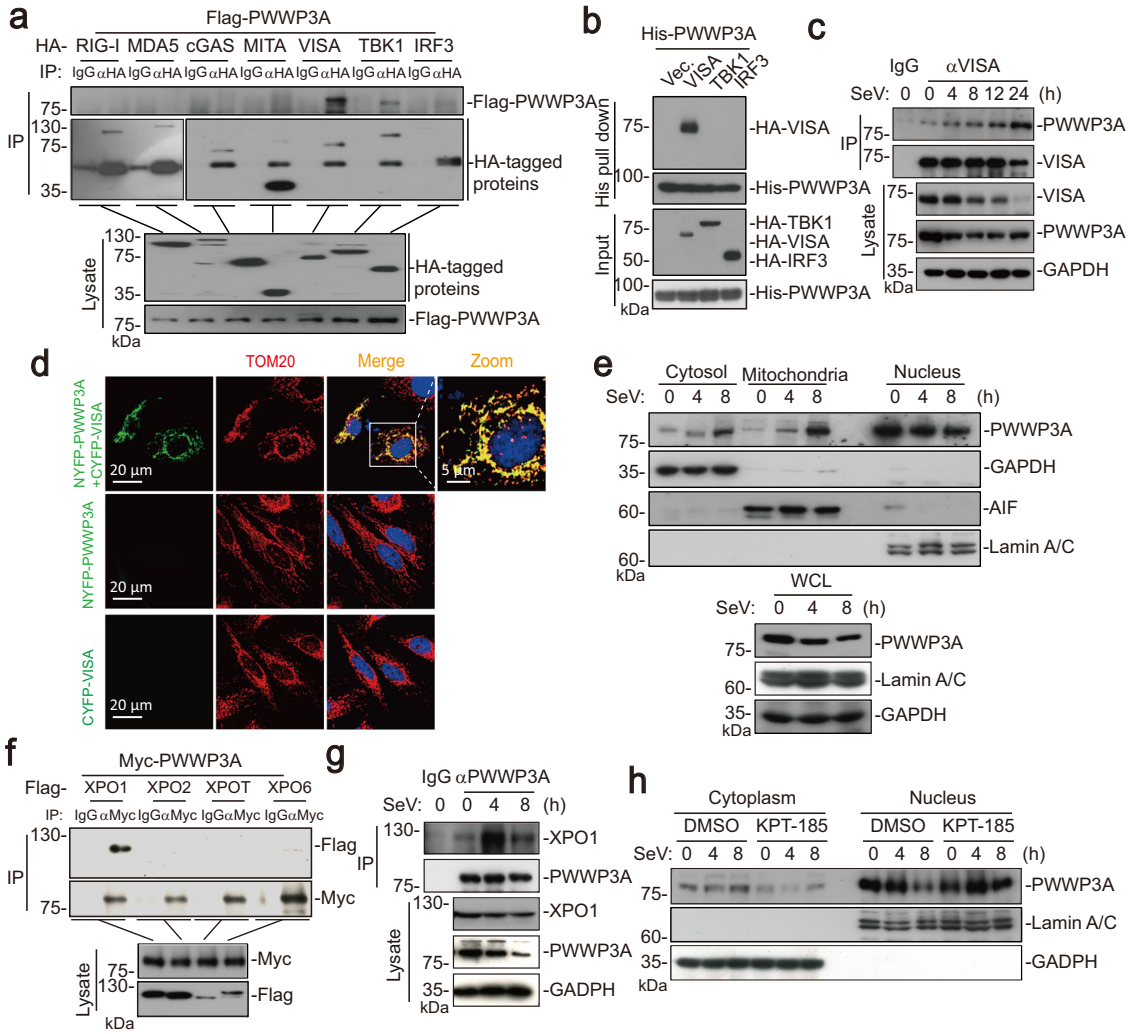

Fig. 5 | PWWP3A translocates to the mitochondria and interacts with VISA. **a** HEK293 cells were transfected with the indicated plasmids. Twenty hours later, co-IP was performed with control IgG or anti-HA. The immunoprecipitates and lysates were analyzed by immunoblotting with anti-HA or anti-Flag. **b** Pull-down and immunoblot analysis of the direct interaction between purified PWWP3A proteins and indicated signaling molecules. HEK293 cells were transfected with the indicated plasmids for 20 h before the cells were lysed and centrifuged, then the supernatants were incubated with *E. coli*-derived His-PWWP3A at 37 °C for 2 h before pull-down assays were performed. **c** HEK293 cells were infected with SeV at the indicated time points, then co-immunoprecipitation was performed with control IgG or anti-VISA. The immunoprecipitates and lysates were analyzed by immunoblotting with indicated antibodies. **d** Confocal microscopy analysis in HEK293 cells transfected with NYFP-PWWP3A and CYFP-VISA for 20 h. Scale bar, 20 μm. **e** The mitochondrial fraction (45%), cytoplasm fraction (20%), nucleus fraction (1%) or whole cell lysates (WCL) from the uninfected or SeV infected HEK293 cells were analyzed by immunoblot analysis with the indicated antibodies. **f** HEK293 cells were transfected with the indicated plasmids. Twenty hours later, co-IP was performed with control IgG or anti-Myc. The immunoprecipitates and lysates were analyzed by immunoblotting with anti-Myc or anti-Flag. **g** HEK293 cells were infected with SeV at the indicated time points, then co-immunoprecipitation was performed with control IgG or anti-PWWP3A. The immunoprecipitates and lysates were analyzed by immunoblotting with indicated antibodies. **h** HEK293 cells treated with KPT-185 (1 μM) for 4 h, followed by the SeV infection at the indicated time points. Then the cytoplasm fraction (20%) and nucleus fraction (1%) from the cells were analyzed by immunoblot analysis with the indicated antibodies. At least three independent experiments were performed with similar results. Source data are provided as a Source Data file.

PWWP3A was predominantly detected in the nucleus, with a minor fraction present in cytosol and mitochondrial fractions (Fig. 5e). Upon SeV infection, the nuclear PWWP3A levels was decreased, accompanied by an increase of PWWP3A in the cytosol and mitochondria (Fig. 5e). Our results indicate that PWWP3A translocates to the mitochondria following SeV infection.

We next investigated the mechanisms underlying the translocation of PWWP3A from the nucleus to the cytoplasm. Initially, we conducted co-IP assays between PWWP3A and several nuclear export proteins, and observed a strong interaction between PWWP3A and XPO1, but not other exportins like XPO2, XPO6, and XPOT (Fig. 5f). Endogenous co-IP experiments further confirmed the PWWP3A-XPO1 association in resting cells, and this association was further enhanced post-viral infection (Fig. 5g). Consistently, the treatment of KPT-185, a XPO1 inhibitor, attenuated SeV-induced nuclear-to-cytoplasmic translocation of PWWP3A (Fig. 5h). In summary, our findings suggest that XPO1 interacts with PWWP3A and facilitates its translocation following SeV infection.

PWWP3A inhibits the recruitment of TBK1 to VISA

It is well established that VISA is phosphorylated by TBK1 and in turn recruits IRF3, thus facilitating TBK1-mediated IRF3 phosphorylation[9]. Notably, our study clearly demonstrated that PWWP3A interacted with VISA and inhibited the phosphorylation of IRF3, but not TBK1, following viral infection. Therefore, we assessed whether PWWP3A attenuates TBK1-mediated phosphorylation of VISA and IRF3. As

https://doi.org/10.1038/s41467-025-59421-x

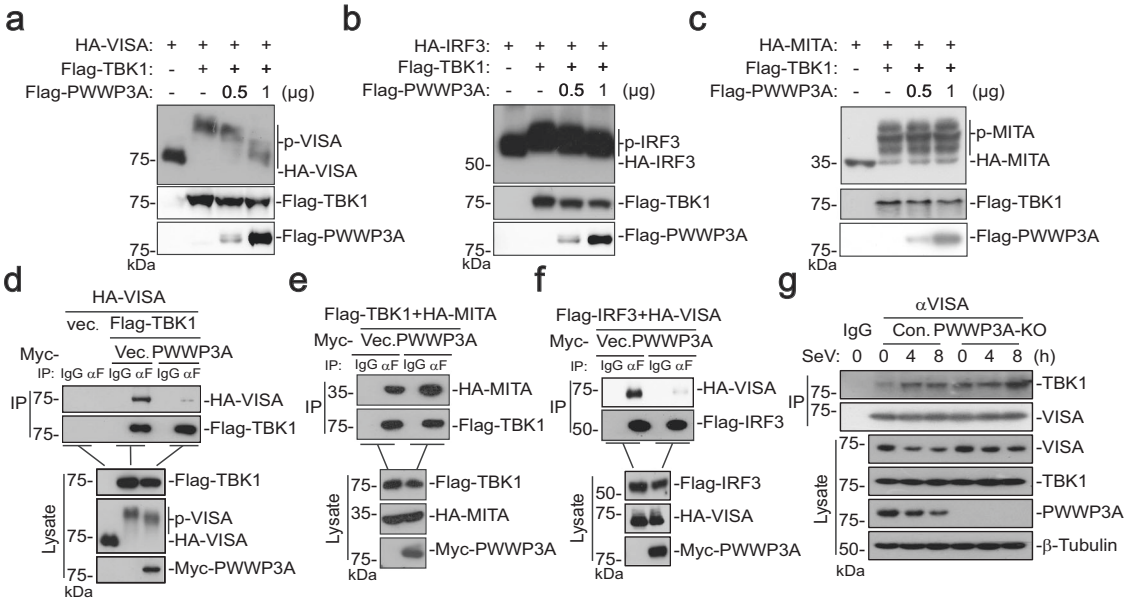

Fig. 6 | PWWP3A inhibits the interaction between TBK1 and VISA. a–c HEK293 cells transfected with the indicated plasmids for 20 h followed by immunoblotting analysis. **d–f** HEK293 cells were transfected with the indicated plasmids. Twenty hours later, co-IP was performed with control IgG or anti-Flag. The immunoprecipitates and lysates were analyzed by immunoblotting with the indicated antibody. **g** The control and PWWP3A- knockout (KO) HEK293 cells were infected with sendai virus (SeV) at the indicated time points, then co-immunoprecipitation was performed with control IgG or anti-VISA. The immunoprecipitates and lysates were analyzed by immunoblotting with indicated antibodies. At least three independent experiments were performed with similar results. Source data are provided as a Source Data file.

shown in Fig. 6a, b, overexpression of PWWP3A markedly impaired the phosphorylation of VISA and IRF3 induced by TBK1. It is reported that MITA, also known as STING, also undergoes phosphorylation by TBK1 to facilitate the following recruitment of IRF3[9,20], and the activated MITA/STING is subject to degradation following viral infection[21]. However, PWWP3A had no effect on TBK1-mediated phosphorylation of MITA, suggesting the specific roles of PWWP3A in the VISA- but not MITA-related signalosome (Fig. 6c).

Having demonstrated that PWWP3A inhibits TBK1-mediated phosphorylation of VISA and IRF3, we subsequently examined whether it reduces the binding of TBK1 to VISA. As expected, PWWP3A specifically diminished the interaction between TBK1 and VISA, while having no impacts on the TBK1-MITA interaction (Fig. 6d, e). Consequently, further recruitment of IRF3 to VISA was also impaired by PWWP3A (Fig. 6f). In contrast, PWWP3A deficiency dramatically enhanced SeV-induced association between VISA and TBK1 compared to control cells (Fig. 6g). These data together show that PWWP3A inhibits VISA-mediated immune signaling by impeding the recruitment of TBK1 to VISA.

PWWP3A competes with TRAF6 to bind to VISA

It has been reported that VISA recruits TBK1 via TRAF proteins, including TRAF2, TRAF3, TRAF5 and TRAF6, which exhibit varying and redundant functionalities across different tissues and cell types[22–25]. Since we identified TRAF6 as a PWWP3A-associated protein in the AP-MS analysis based on Myc-tagged PWWP3A transfected cells (Fig. 7a), we thus assessed whether PWWP3A utilizes TRAF6 to interfere with the binding of TBK1 to VISA. To this end, we initiated our investigation by examining the interactions between PWWP3A and individual TRAF proteins. In the in vitro pull-down assays, PWWP3A displayed direct interaction solely with TRAF6, while no significant interactions were observed with TRAF2, TRAF3 or TRAF5 (Fig. 7b). Endogenous co-IP experiments demonstrated an interaction between PWWP3A and TRAF6 in resting cells, with a substantial enhancement of this interaction observed post-viral infection (Fig. 7c).

Furthermore, we examined whether PWWP3A affects the interaction between TRAF6 and VISA. Co-IP assays suggested that overexpressed PWWP3A specifically disrupted the interaction between VISA and TRAF6 (Fig.7d), while leaving the interactions of VISA with TRAF2, TRAF3, and TRAF5 unaffected (Supplementary Fig. 8a, b). Additional pull-down assays confirmed that PWWP3A significantly hindered the VISA-TRAF6 association in vitro (Fig. 7e). Endogenous co-IP assays revealed that viral infection induced the formation of the VISA-TRAF6 complex in wild-type cells, with a pronounced enhancement observed in PWWP3A-KO cells (Fig. 7f). Collectively, these experiments demonstrate that PWWP3A specifically disrupts the interaction between VISA and TRAF6.

We further generated TRAF6-deficient HEK293 cells by CRISPR/Cas9 methods and examined the potential role of PWWP3A in regulating virus-triggered signaling via TRAF6 (Supplementary Fig. 9a). RT-qPCR assays revealed that overexpression of PWWP3A significantly suppressed the transcription of downstream effector genes induced by SeV in wild-type cells, whereas this inhibitory effect was absent in TRAF6-deficient cells (Supplementary Fig. 9a). Consistently, overexpression of PWWP3A notably impaired the SeV-triggered phosphorylation of IRF3 in wild-type cells, but this effect was attenuated upon the deficiency of TRAF6 (Supplementary Fig. 9b). The inhibitory ability of PWWP3A on TBK1-VISA association was abolished in TRAF6-deficient cells as well (Supplementary Fig. 9c). These data collectively suggest that PWWP3A regulates virus-triggered signaling pathways by preventing the recruitment of TRAF6 to VISA.

It is reported that the glutamic acids (E) 155 and 457 of VISA are two TRAF6 binding sites[7], we constructed the VISA-d6 mutant, in which both the E155 and E457 of VISA were mutated to aspartic acid (D), rendering it unable to bind to TRAF6 (Fig. 7g). Interestingly, the co-IP experiments revealed that the VISA-d6 mutant failed to interact with PWWP3A (Fig. 7h), and the similar results were obtained in the in vitro pull-down assays (Fig. 7i). These results suggest that PWWP3A binds to the TRAF6-binding sites of VISA, thereby competing with TRAF6 for binding to VISA. In conclusion, our experiments demonstrate that PWWP3A inhibits the recruitment of TBK1 to VISA by disrupting the formation of the VISA-TRAF6-TBK1 complex.

https://doi.org/10.1038/s41467-025-59421-x

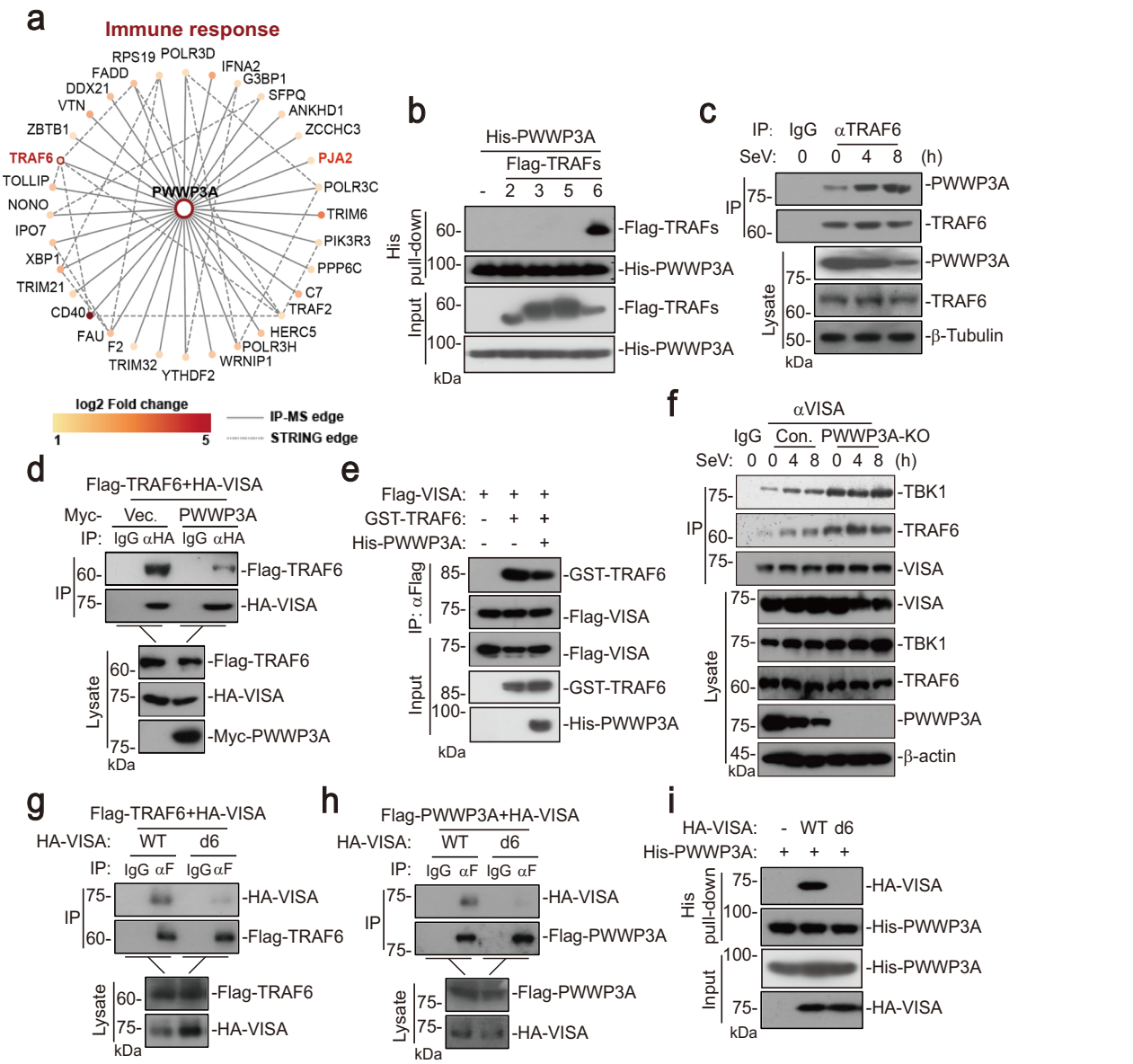

Fig. 7 | PWWP3A competes with TRAF6 to bind to VISA. a Protein–protein interaction (PPI) map for PWWP3A and immune response related interactors. **b** HEK293 cells were transfected with the indicated plasmids for 20 h before the cells were lysed and centrifuged, then the supernatants were incubated with *E. coli*-derived His-PWWP3A at 37 °C for 2 h before pull-down assays were performed. **c** HEK293 cells were infected with sendai virus (SeV) at the indicated time points, then co-immunoprecipitation was performed with control IgG or anti-TRAF6. The immunoprecipitates and lysates were analyzed by immunoblotting with indicated antibodies. **d** HEK293 cells were transfected with the indicated plasmids. Twenty hours later, co-IP was performed with control IgG or anti-HA. The immunoprecipitates and lysates were analyzed by immunoblotting with the indicated antibody. **e** The Flag-VISA expressed cell lysate was incubated with *E. coli*-derived GST-TRAF6 at 37 °C for 2 h before co-IP analysis. **f** The control and PWWP3A-knockout (KO) HEK293 cells were infected with SeV at the indicated time points, then co-immunoprecipitation was performed with control IgG or anti-VISA. The immunoprecipitates and lysates were analyzed by immunoblotting with indicated antibodies. **g**, **h** HEK293 cells were transfected with the indicated plasmids. Twenty hours later, co-IP was performed with control IgG or anti-Flag. The immunoprecipitates and lysates were analyzed by immunoblotting with the indicated antibody. **i** The pull-down assay was performed as described in (**b**) except HA-VISA and its mutant (VISA-d6) were used here. VISA-d6, the mutant of VISA in which both the E155 and E457 of VISA were mutated to aspartic acid (D). At least three independent experiments were performed with similar results. Source data are provided as a Source Data file.

Discussion

PWWP3A was originally discovered as a DNA repair factor which is recruited to the DNA damage sites by TP53BP1 and facilitates efficient DNA repair[11]. Recently, we identified that aged *Pwwp3a*$^{-/-}$ male mice exhibit testicular atrophy, potentially due to alterations in the immune microenvironment[12]. However, the research on PWWP3A is currently constrained, and its functions in diverse physiological and pathological contexts remain unclear. Herein, we identify PWWP3A as a down-regulated protein which negatively regulates the innate immune response to RNA viruses, specifically by competing with TRAF6 for binding to VISA on mitochondria. This competition inhibits the recruitment of TBK1 and subsequent phosphorylation of IRF3 (Fig. 8).

Multiple lines of evidence suggest that PWWP3A expression is suppressed during RNA viral infection. Firstly, by utilizing TMT-based quantitative proteomics, which offer unique insights into the protein regulatory network compared to conventional transcriptome studies[26], we observed a decrease in PWWP3A protein levels following SeV infection. Secondly, we demonstrated that RNA viruses SeV and VSV, but not the DNA virus HSV-1, induce the degradation of PWWP3A, which was reversible with the proteasome inhibitor MG132. These

https://doi.org/10.1038/s41467-025-59421-x

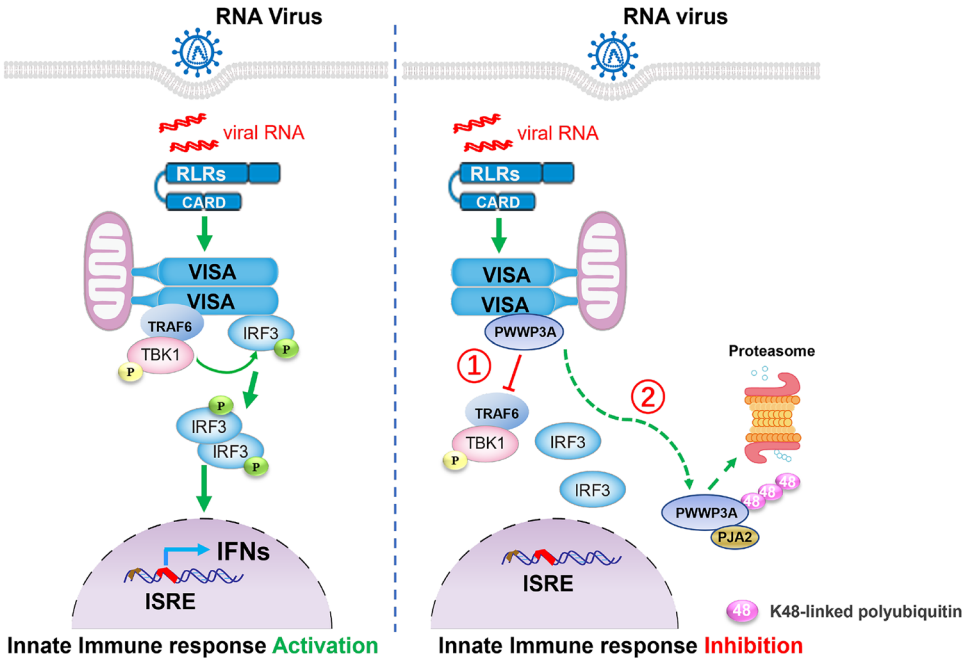

Fig. 8 | A model on PWWP3A-mediated inhibition of antiviral innate immune signaling. Upon binding to viral dsRNA, RIG-I undergoes a conformational change and releases its N-terminal tandem CARD domain, which further recruits to the mitochondrial adaptor protein VISA/MAVS. VISA polymers then recruit TBK1 through different TRAF proteins, which in turn phosphorylates VISA. Phosphorylated VISA recruits IRF3 for phosphorylation through TBK1, consequently inducing the induction of type I IFNs. PWWP3A acts as a binding partner of VISA, thereby specifically inhibiting the recruitment of TBK1-TRAF6 to the VISA signalosome, which further inhibits the IRF3 phosphorylation and IFNs induction following virus infection (i). However, the degree of PWWP3A-mediated inhibition could be regulated by PJA2-mediated PWWP3A degradation after virus infection (ii). Despite a reduction in its overall abundance due to viral infection, PWWP3A still localizes to mitochondria and interacts with VISA to maintain its inhibitory effect.

findings imply that RNA virus induces the degradation of PWWP3A in a proteasome-dependent manner. Notably, we observed a decrease in PWWP3A expression from 4 to 12 h post-SeV infection, followed by the gradual restoration after 24 h. By utilizing the AP-MS, we further identified PJA2 as an E3 ligase that interacted with PWWP3A upon viral infection and mediated its K48-linked polyubiquitination and the subsequent degradation.

PWWP3A has been implicated in regulating the DNA damage repair, yet its role in other physiological and pathological processes remain largely unknown. Here, we demonstrate that PWWP3A specifically inhibits RLRs-mediated innate immune response against RNA viruses. Overexpression of PWWP3A suppressed the induction of *IFNB1* and other downstream antiviral effectors triggered by SeV. While deficiency of PWWP3A enhanced the transcription of these antiviral genes triggered by SeV, VSV, or cytoplasmic-transfected dsRNA in both HEK293 cells and murine primary cells. In contrast, PWWP3A exerted minimal effects on immune signaling triggered by DNA virus or mediated by TLR3. In accordance with these findings, the replication of VSV and SARS-CoV-2, but not HSV-1, was reduced in PWWP3A-deficient cells. Furthermore, *Pwwp3a*$^{-/-}$ mice exhibited elevated levels of serum antiviral cytokines and greater resistance to RNA virus, but not DNA virus, compared to their wild-type littermates. These results collectively demonstrate that PWWP3A specifically inhibits the innate immune response to RNA viruses, thereby enhancing our understanding of PWWP3A's multifaceted functions.

Upon recognizing viral RNA, RIG-I induces VISA to form prion-like aggregates on the outer mitochondrial membrane. VISA then recruits TBK1, which, in turn, phosphorylates VISA. Phosphorylated VISA then recruits IRF3, allowing for its activation by TBK1. In this study, we found that PWWP3A translocated from the nucleus to the mitochondria and interacted with VISA. This interaction negatively regulated the antiviral innate immune response by blocking TBK1 recruitment to the VISA signalosome, thus inhibiting IRF3 phosphorylation. Previously, TBK1 was proposed to be constitutively associates with TRAFs in resting cells, and then translocates to VISA for its phosphorylation[7]. Consistently, we found that VISA deficiency abolished SeV-triggered phosphorylation of TBK1 and IRF3 (Supplementary Fig. 10). Interestingly, the reintroduction of TRAF3 and TRAF6 dramatically rescued the phosphorylation of TBK1, but not IRF3, in VISA-deficient cells (Supplementary Fig. 10). These experiments suggest that TBK1 is activated by TRAF6 prior its recruitment to VISA following virus infection, and TBK1 activation alone is insufficient to activate IRF3 in the absence of VISA.

Additionally, our results showed that overexpression of PWWP3A impaired IRF3 phosphorylation induced by SeV in control cells, but this effect was attenuated in TRAF6-KO cells, indicating that PWWP3A inhibited TRAF6-mediated activation of IRF3. AP-MS screening and the further in vivo and in vitro experiments demonstrated that PWWP3A competed with TRAF6 for binding to VISA, whereas deficiency of PWWP3A significantly increased the recruitment of the TRAF6-TBK1 complex to VISA after viral infection. The residues E115 and E457 of VISA, which are critical for mediating the TRAF6-VISA association[7], were also essential for its interaction with PWWP3A. Notably, we observed an enhanced interaction between TRAF6 and PWWP3A upon viral infection, which may also contribute to PWWP3A-mediated disruption of VISA signalosome. Individual TRAF proteins have been reported to play either redundant or distinct roles across diverse tissues and cells[7]. Our study thus uncovers a specific mechanism through which PWWP3A specifically regulates TRAF6-mediated signaling in response to RNA virus infection.

The innate antiviral immune response plays a pivotal role in the host defense against viral infections. However, its dysregulation, either excessive or insufficient, significantly compromise host health. Even during the initial phases of RNA virus infection, the VISA-mediated innate immune response requires intricate spatial and temporal regulation by various inhibitors, such as USP21, WDR77, NLRP11 or

TRAF3IP3[27–30]. Here, we identify PWWP3A as a negative regulator of VISA, which partially relocates to the mitochondria and attenuates the immune response following viral infection. This mechanism ensures timely, suitable, and controlled orchestration of the innate immune response. However, the degree of PWWP3A-mediated inhibition of immune response could be modulated by its degradation. Specifically, at the early stages of RNA virus infection, the PWWP3A protein level decreases, thereby alleviating its suppressive effect on the innate immune response. It's worth noting that, despite a decrease in its overall protein levels following viral infection, PWWP3A still localizes to mitochondria and interacts with VISA to maintain its inhibitory effect. While during the later phase of viral infection, PWWP3A expression is restored, thus inhibiting overactivation of the VISA signalosome more efficiently to prevent excessive and detrimental immune responses. In summary, we uncover the important role of PWWP3A in inhibiting the innate immune response to RNA viruses. This finding contributes to our understanding of the complex functions of PWWP3A and its potential implications in human health and disease.

Methods

Ethics statement and mice

The animal care and use were adhered to the Chinese National Guidelines for Ethical Review of Animal Welfare. The protocols and procedures for mice experiments in this study was approved by the College of Life Sciences Animal Care and Use Committee of Wuhan University (WDSKY0202009). The *Pwwp3a*$^{flox/flox}$ mice were generated by targeted embryonic stem cells and blastocyst injections previously[12]. Briefly, the *Pwwp3a*-targeting vector was constructed with a 475 bp genomic DNA fragment containing exon4 which was flanked by loxp sites. The two homologous arms (LHA: 1829bp, RHA: 1806bp) were amplified from testicular genome of mouse. Then, the linearized targeting vector was electroporated into V6.5 embryonic stem (ES) cells (a kind gift from prof. P. Jeremy Wang at University of Pennsylvania). Targeted ES cells were screened and then injected into C57BL/6J blastocysts and subsequently transferred to the uteruses of pseudopregnant ICR females. The *Pwwp3a*^{flox} allele was transmitted from chimeric males. To obtained *Pwwp3a*$^{+/-}$ mice, we used *Stra8*-cre to mediate the deletion of flox allele (*Stra8 GFP*-cre mice from prof. Minghan Tong at University of Chinese Academy of Sciences). In this study, we performed *Pwwp3a*$^{+/-}$ male backcrossing with WT female mice for three generations before obtaining *Pwwp3a* KO mice for subsequent experiments (Supplementary Fig. 4). *V5-Pwwp3a* KI mice were generated by the CRISPR-Cas9 technology[12,31]. The *V5*-linker donor sequence was inserted the *Pwwp3a* genomic locus after ATG. We designed two sgRNAs for ensuring accuracy (KI-sgRNA1: GCATCCGTCATGACTCAGAAAGG; KI-sgRNA2: TACTCCTTTCTGAGTCATGACGG). *Pwwp3b*$^{flox/Y}$ mice were purchased from GemPharmatech Company, China. Then, they were crossed with *Stra8 GFP*-cre mice to obtain *Pwwp3b* KO mice. C57BL/6 J and ICR mice were bought from Beijing Vital River Laboratory Animal Technology Co., Ltd (Beijing, China). All mice were bred at a specific pathogen-free facility (SPF) with temperature at 22 °C to 24 °C, relative humidity at 50% to 60% and light/dark cycle at 12/12 h. The primers used for genotyping are provided in the Supplementary Table 1.

Preparation of BMDMs

Bone marrow cells were isolated from tibiae and femur of male C57BL/6J mice (8–10-week-old), and were then cultured in RPMI 1640 medium supplemented with 10% FBS and recombinant murine M-CSF-containing conditional medium for 5 days for generation of BMDMs.

Preparation of MLFs

The lungs of male C57BL/6J mice (8–10-week-old) were minced, which were then digested with type II collagenase (10 μg/mL) and DNase I (20 μg/mL) in calcium and magnesium free HBSS at 37 °C for 3 h with shaking. Cell suspensions were sequentially filtered through 100 μm and 40 μm cell strainers, which were then centrifuged at 200 × *g* for 4 min. The pelleted cells were then cultured in 100 mm dishes in DMEM medium supplemented with 10% fetal bovine serum (FBS) and 1% penicillin- streptomycin. One hour later, the adherent fibroblasts were washed with HBSS and then cultured in the above medium.

Cell culture

HEK293 cells (GDC0187) and immortalized MLFs (GPC0382) were obtain from the China Center for Type Culture Collection (CCTCC). Caco2-N cells were provided by Dr. Qiang Ding (Tsinghua University, China)[18]. The cells were cultured in Dulbecco's Modified Eagle's Medium (DMEM) supplemented with 10% FBS and 1% penicillin- streptomycin. HIOECs were provided by Dr. Huan Liu (Wuhan University, China)[32]. HIOECs were grown in Defined K-SFM Keratinocyte Serum Free Medium (2894708, Gibco, Thermo Fisher Scientific Inc., MA). Additionally, weekly PCR analyses was conducted using primers targeting mycoplasma DNA to confirm the absence of mycoplasma contamination. The primers used for PCR are provided in the Supplementary Table 1.

Virus preparation and infection

The SeV and PR8 viruses were propagated in the 10-day-old SPF chicken embryonated eggs. HSV-1 was routinely propagated in the Vero cells, while the VSV virus was propagated in the BHK-21 cells. These viruses were purified and transferred to a temperature of −80 °C for long-term storage or utilized in infection experiments. The titer of VSV or HSV-1 was measured by plaque assay using BHK-21 or Vero cells; the titer of PR8 virus was measured by EID50 assay and SeV virus particles was measured by hemagglutination test[33–36]. Additionally, PCR analysis of the viruses were conducted using primers targeting mycoplasma DNA to confirm the absence of mycoplasma contamination. Cells were infected with SeV (MOI = 1), VSV (MOI = 0.1), EMCV (MOI = 0.1) or HSV-1 (MOI = 0.1). *Pwwp3a*$^{+/+}$ and *Pwwp3a*$^{-/-}$ mice were intravenous injected with VSV (2×10^7 PFU per mouse) or HSV-1 (2×10^7 PFU per mouse)[37,38]. PR8 (10^6 EID50) was diluted in PBS and intranasally administered to anesthetized mice.

Reagents

The reagents and antibodies used in this study are provided in the Supplementary Table 2. All antibodies used in this study are from commercial suppliers who have verified the specificity of the antibodies by using transfected proteins or knockout cell lines.

Constructs

Flag- or Myc-tagged PWWP3A and their mutants were constructed in the pRK vector, GST-tagged TRAF6 were constructed in the pGEX vector and His-tagged PWWP3A were constructed in the pET-28a vector by standard molecular biology protocols. The NYFP-PWWP3A and CYFP-VISA plasmids were constructed as follows: the NYFP (consisting of amino acids 1-173 of mVenus) was cloned into the pRK vector, and then the mammalian *PWWP3A* cDNA was cloned following NYFP tag. Similarly, to generate the CYFP-VISA construct, CYFP (consisting of amino acids 155-239 of mVenus) was also cloned into the pRK vector, and then the mammalian *VISA* cDNA was cloned following CYFP tag. pRK vector-based mammalian expression plasmids for Flag- or HA-tagged VISA and its mutants, TRAF2, TRAF3, TRAF5, TRAF6, RIG-I, MDA5, cGAS, MITA, IRF3 and TBK1, and the IFN-β, IRF1 promoter and ISRE reporter plasmid were obtained from Dr. Hong-bing Shu (Wuhan University)[39,40]. The plasmids encoding the E3 ligases involved in this study were purchased from Miaoling bio. Inc. (Wuhan, China).

TMT-based proteomics

The BMDMs were infected with SeV at the indicated time points, then the cells were harvested from 10 cm dish (about 10^7 cells) and freeze-dried ($n = 2$ biological replicates per group). Proteomic sample preparation and TMT labeling were performed on cell samples as described in the previous study and detailed below[41]. Briefly, dried samples were redissolved in 30 μL lysis buffer (6 M urea/2 M thiourea in triethylammonium bicarbonate buffer (TEAB), Sigma, USA), reduced by Tris (2 carboxyethyl) phosphine (TCEP, Sigma), alkylated by iodoacetamide (IAA, Sigma) and digested by Lys-C (Hualishi Tech, Cat # HLS LYS001C) and trypsin (Hualishi Tech, Cat # HLS TRY001C) assisted by pressure cycling technology (PCT). Clean peptides were labeled by TMT regent (Thermo Fisher Scientific, Cat# A44520, Lot # VL313890) and separated on Thermo Ultimate Dinex 3000 (Thermo Fisher Scientific, San Jose, USA) with an XBridge Peptide BEH C18 column (300 Å, 5 μm × 4.6 mm × 250 mm) (Waters, Milford, MA, USA) using a 96 min LC gradient from 5% to 35% acetonitrile (ACN) in 10 mM ammonia (pH = 10.0) at a flow rate of 1 mL/min to 60 fractions.

The fractions were combined using the following strategy: 1) firstly combine the 1st to 4th and 14th to 18th as the new 1st fraction; 2) combine the 5th to 13rd as the new 2nd fraction; 3) combine the left 80 fractions with equal distances (eg. 1st and 41st, 2nd and 42nd). Together, we got 40 combinations of fractions and dried them in vacuum.

Dry peptides were re-dissolved and analyzed by a Q Exactive HF-X hybrid Quadrupole-Orbitrap with the same LC-MS/MS settings as described previously[41]. Acquired MS raw data were analyzed by Proteome Discoverer (Version 2.4.1.15, Thermo Fisher Scientific) using a FASTA file of 17,000 reviewed mouse protein entries (downloaded from Uniprot at 17th Jan, 2020).

Affinity purification-mass spectroscopy (AP-MS)

HEK293 cells (about 3×10^7 cells) were transfected with plasmid encoding PWWP3A-Myc or empty control vector. Twenty-four hours later, the co-IP assays were performed using anti-Myc antibody ($n = 3$ biological replicates per group). Subsequently, beads samples obtained from co-IP were incubated in the reaction buffer (1% SDC, 100 mM Tris-HCl, 10 mM TCEP, 40 mM CAA, pH = 8.5) at 95 °C for 10 min for protein denaturation, cysteine reduction and alkylation, followed by trypsin digestion overnight. The digested peptides were desalted and then loaded onto a timsTOF Pro mass spectrometer (Bruker Daltonics) coupled with an UltiMate 3000 RSLC nano-system (Thermo Fisher Scientific) and analyzed in diaPASEF mode, using the DIA-MN software (V1.9.1). The capillary voltage was set to 1400 V. The MS and MS/MS spectra were acquired from 100 to 1700 m/z. The ion mobility was scanned from 0.6 to 1.6 Vs/cm^2. The accumulation time and ramp time were set to 100 ms.

The raw DIA data were searched against the reviewed human database from UniProt (2024-08-07, 20654 entries) using DIA-NN software (V1.9.1) in library-free mode. Enriched proteins with a fold change >2 and p value < 0.05 between groups of PWWP3A-Myc and control vector were screened out as candidate interactors of PWWP3A. Functional annotations were performed using GO and KEGG databases. Protein-protein interaction networks were constructed and analyzed using the STRING database and visualized with Cytoscape software[42,43].

CRISPR-Cas9-mediated gene editing

Genome engineering was performed by using the CRISPR-Cas9 system[44,45]. Double-stranded oligonucleotides corresponding to the target sequences were cloned into the lenti-CRISPR-V2 vector and co-transfected with psPAX2 and pMD2.G into HEK293 cells. Two days after transfection, the viruses were harvested to infect HEK293 cells or MLFs. The infected cells were selected with puromycin (1 μg/mL) for at least 7 days to obtain PWWP3A-, PJA2-, and TRAF6-KO cell pools. The gRNA sequences for each gene are provided in the Supplementary Table 1.

Confocal microscopy

HEK293 cells were transfected with the indicated plasmids for 20 h, and then fixed with 4% paraformaldehyde for 10 min, and permeabilized with 0.1% Triton X-100 in PBS for 15 min. The cells were blocked with 1% BSA in PBS for 1 h. Cells were then incubated with primary antibodies overnight at 4 °C. Alexa Fluor 594-conjugated secondary antibodies were incubated for 1 h. The nuclei were stained with DAPI for 2 min before images were acquired using a Leica SP8 confocal microscope (Leica, Germany) with the 60× objective, using Leica Application Suite X (3.7.4.23463) software.

Co-IP and immunoblot analysis

Cells were lysed in 1 mL NP-40 lysis buffer (20 mM Tris-HCl, pH 7.4-7.5, 150 mM NaCl, 1 mM EDTA, 1% NP-40, 10 μg/mL aprotinin, 10 μg/mL leupeptin and 1 mM PMSF). The lysate was centrifuged at 13,800 × g for 10 min at 4 °C. For each immunoprecipitation, the supernatant was incubated with 0.5 μg of the indicated antibody and 35 μL of 50% slurry of GammaBind G Plus-Sepharose at 4 °C for 2 h. The beads were then washed for three times with 1 mL lysis buffer containing 500 mM NaCl. The bound proteins were separated by SDS-PAGE and the associated proteins were analyzed by immunoblot analysis. Images for immunoblots were obtained using EPSON Scan (3.9.2. OSC), and quantified using the Chemiluminescence-Imaging (3.2.1.0) software.

Subcellular fractionation

Cell fractionation experiments were performed as previously described with modification[46]. In brief, cells were left un-infected or infected with SeV at the indicated time points, the cells were then washed with PBS and lysed by douncing 40 times in 1 mL of homogenization buffer (10 mmol/L Tris-HCl, pH 7.4, 2 mmol/L $MgCl_2$, 10 mmol/L KCl, 250 mmol/L sucrose). The homogenized samples were centrifuged at 500 × g for 10 min to collect the pellet as the crude nucleus. The supernatants were centrifuged at 5000 × g for 10 min to precipitate crude mitochondria and cytosol fractions.

Transfection and reporter assays

The cells were transfected by standard calcium phosphate precipitation. To normalize for transfection efficiencies, pRL-TK (*Renilla* luciferase) reporter plasmid (0.1 μg) was added to each transfection. Empty control plasmid was added to ensure that each transfection received the same amount of total plasmid DNA. Twenty hours after transfection, cells were treated or left untreated with the indicated stimuli before luciferase assays were performed using a dual-specific luciferase assay kit. Firefly luciferase activities were normalized based on *Renilla* luciferase activities.

RT-qPCR analysis

Total RNA was isolated for RT-qPCR analysis to measure mRNA levels of the indicated genes according to the manufacturer's protocol of RNAiso Plus. The qPCR data were collected using q225 (19.12.0201) software. Data shown are the relative abundance of the indicated mRNA derived from human or mouse cells normalized to that of *GAPDH* or *Gapdh*. The sequences of qPCR primers are provided in the Supplementary Table 1.

Statistical analysis

Comparisons between two groups with normally distributed variables were analyzed using a two-tailed, unpaired Student's t test, while multiple comparisons were analyzed by one-way ANOVA without adjustment, by using GraphPad Prism (8.4.0.671). $p < 0.05$ was considered significant. For animal survival analysis, the Kaplan-Meier method was adopted to generate graphs, and the survival curves were analyzed with log-rank analysis. Other graphs are shown as mean ± SD.

Reporting summary

Further information on research design is available in the Nature Portfolio Reporting Summary linked to this article.

Data availability

All data relating to this study can be found in the maintext, figures or supplementary information. The protein mass spectrometry raw data generated in this study have been deposited in the PRIDE database under accession codes PXD051098 and PXD058791. Source data are provided with this paper.

References

1. Hu, M. M. & Shu, H. B. Cytoplasmic mechanisms of recognition and defense of microbial nucleic acids. *Annu Rev. Cell. Dev. Biol.* **34**, 357–379 (2018).
2. Rothenfusser, S. et al. The RNA helicase Lgp2 inhibits TLR-independent sensing of viral replication by retinoic acid-inducible gene-I. *J. Immunol.* **175**, 5260–5268 (2005).
3. Yoneyama, M. et al. The RNA helicase RIG-I has an essential function in double-stranded RNA-induced innate antiviral responses. *Nat. Immunol.* **5**, 730–737 (2004).
4. Seth, R. B., Sun, L., Ea, C. K. & Chen, Z. J. Identification and characterization of MAVS, a mitochondrial antiviral signaling protein that activates NF-kappaB and IRF 3. *Cell* **122**, 669–682 (2005).
5. Xu, L. G. et al. VISA is an adapter protein required for virus-triggered IFN-beta signaling. *Mol. Cell* **19**, 727–740 (2005).
6. Hou, F. et al. MAVS forms functional prion-like aggregates to activate and propagate antiviral innate immune response. *Cell* **146**, 448–461 (2011).
7. Fang, R. et al. MAVS activates TBK1 and IKKepsilon through TRAFs in NEMO dependent and independent manner. *PLoS Pathog.* **13**, e1006720 (2017).
8. Liu, S. et al. MAVS recruits multiple ubiquitin E3 ligases to activate antiviral signaling cascades. *Elife* **2**, e00785 (2013).
9. Liu, S. et al. Phosphorylation of innate immune adaptor proteins MAVS, STING, and TRIF induces IRF3 activation. *Science* **347**, aaa2630 (2015).
10. Wu, H. et al. Structural and histone binding ability characterizations of human PWWP domains. *PLoS One* **6**, e18919 (2011).
11. Huen, M. S. et al. Regulation of chromatin architecture by the PWWP domain-containing DNA damage-responsive factor EXPAND1/MUM1. *Mol. Cell* **37**, 854–864 (2010).
12. Chen, Z. et al. PWWP3A deficiency accelerates testicular senescence in aged mice. *Andrology* https://doi.org/10.1111/andr.13774 (2024).
13. Liu, H. et al. Nuclear cGAS suppresses DNA repair and promotes tumorigenesis. *Nature* **563**, 131–136 (2018).
14. Crossley, M. P. et al. R-loop-derived cytoplasmic RNA-DNA hybrids activate an immune response. *Nature* **613**, 187–194 (2023).
15. Marzio, A. et al. EMSY inhibits homologous recombination repair and the interferon response, promoting lung cancer immune evasion. *Cell* **185**, 169–183.e119 (2022).
16. Liu, R. et al. Innate immune response orchestrates phosphoribosyl pyrophosphate synthetases to support DNA repair. *Cell Metab.* **33**, 2076–2089.e2079 (2021).
17. Dikic, I. Proteasomal and autophagic degradation systems. *Annu Rev. Biochem* **86**, 193–224 (2017).
18. Ju, X. et al. A novel cell culture system modeling the SARS-CoV-2 life cycle. *PLoS Pathog.* **17**, e1009439 (2021).
19. Xu, Y. et al. A cell-based high-content screen identifies isocotoin as a small molecule inhibitor of the meiosis-specific MEIOB-SPATA22 complex. *Biol. Reprod.* **103**, 333–342 (2020).
20. Zhong, B. et al. The adaptor protein MITA links virus-sensing receptors to IRF3 transcription factor activation. *Immunity* **29**, 538–550 (2008).
21. Hu, M. M. et al. Sumoylation promotes the stability of the DNA sensor cGAS and the adaptor STING to regulate the kinetics of response to DNA virus. *Immunity* **45**, 555–569 (2016).
22. Brink, R. & Lodish, H. F. Tumor necrosis factor receptor (TNFR)-associated factor 2A (TRAF2A), a TRAF2 splice variant with an extended RING finger domain that inhibits TNFR2-mediated NF-kappaB activation. *J. Biol. Chem.* **273**, 4129–4134 (1998).
23. Hacker, H. et al. Specificity in Toll-like receptor signalling through distinct effector functions of TRAF3 and TRAF6. *Nature* **439**, 204–207 (2006).
24. Hacker, H., Tseng, P. H. & Karin, M. Expanding TRAF function: TRAF3 as a tri-faced immune regulator. *Nat. Rev. Immunol.* **11**, 457–468 (2011).
25. Izban, K. F., Ergin, M., Martinez, R. L. & Alkan, S. Expression of the tumor necrosis factor receptor-associated factors (TRAFs) 1 and 2 is a characteristic feature of Hodgkin and Reed-Sternberg cells. *Mod. Pathol.* **13**, 1324–1331 (2000).
26. Vasaikar, S. et al. Proteogenomic analysis of human colon cancer reveals new therapeutic opportunities. *Cell* **177**, 1035–1049 e1019 (2019).
27. Fan, Y. et al. USP21 negatively regulates antiviral response by acting as a RIG-I deubiquitinase. *J. Exp. Med.* **211**, 313–328 (2014).
28. Li, J. et al. WDR77 inhibits prion-like aggregation of MAVS to limit antiviral innate immune response. *Nat. Commun.* **14**, 4824 (2023).
29. Qin, Y. et al. NLRP11 disrupts MAVS signalosome to inhibit type I interferon signaling and virus-induced apoptosis. *EMBO Rep.* **18**, 2160–2171 (2017).
30. Deng, M. et al. TRAF3IP3 negatively regulates cytosolic RNA induced anti-viral signaling by promoting TBK1 K48 ubiquitination. *Nat. Commun.* **11**, 2193 (2020).
31. Zhan, J., Cui, P., Yu, Z., Qu, W. & Luo, M. SDX on the X chromosome is required for male sex determination. *Cell Res.* **32**, 99–102 (2022).
32. Xiao, Y. et al. Chromatin conformation of human oral epithelium can identify orofacial cleft missing functional variants. *Int. J. Oral. Sci.* **14**, 43 (2022).
33. Huang, J. et al. SIKE is an IKK epsilon/TBK1-associated suppressor of TLR3- and virus-triggered IRF-3 activation pathways. *EMBO J.* **24**, 4018–4028 (2005).
34. Zhang, B. et al. The nucleoprotein of influenza A virus inhibits the innate immune response by inducing mitophagy. *Autophagy* **19**, 1916–1933 (2023).
35. Xu, J. et al. Replication defective viral genomes exploit a cellular pro-survival mechanism to establish paramyxovirus persistence. *Nat. Commun.* **8**, 799 (2017).
36. Tapia, K. et al. Defective viral genomes arising in vivo provide critical danger signals for the triggering of lung antiviral immunity. *PLoS Pathog.* **9**, e1003703 (2013).
37. Song, G. et al. E3 ubiquitin ligase RNF128 promotes innate antiviral immunity through K63-linked ubiquitination of TBK1. *Nat. Immunol.* **17**, 1342–1351 (2016).
38. Li, S. Z. et al. Phosphorylation of MAVS/VISA by Nemo-like kinase (NLK) for degradation regulates the antiviral innate immune response. *Nat. Commun.* **10**, 3233 (2019).
39. Xu, Y. R. et al. Tankyrases inhibit innate antiviral response by PARylating VISA/MAVS and priming it for RNF146-mediated ubiquitination and degradation. *Proc. Natl. Acad. Sci. USA* **119**, e2122805119 (2022).
40. Lei, C. Q. et al. FoxO1 negatively regulates cellular antiviral response by promoting degradation of IRF3. *J. Biol. Chem.* **288**, 12596–12604 (2013).
41. Nie, X. et al. Multi-organ proteomic landscape of COVID-19 autopsies. *Cell* **184**, 775–791 e714 (2021).
42. Bouhaddou, M. et al. SARS-CoV-2 variants evolve convergent strategies to remodel the host response. *Cell* **186**, 4597–4614 e4526 (2023).

43. Dai, S. et al. Interactome profiling of Crimean-Congo hemorrhagic fever virus glycoproteins. *Nat. Commun.* **14**, 7365 (2023).
44. Sanjana, N. E., Shalem, O. & Zhang, F. Improved vectors and genome-wide libraries for CRISPR screening. *Nat. Methods* **11**, 783–784 (2014).
45. Shalem, O. et al. Genome-scale CRISPR-Cas9 knockout screening in human cells. *Science* **343**, 84–87 (2014).
46. Lei, C. Q. et al. ECSIT bridges RIG-I-like receptors to VISA in signaling events of innate antiviral responses. *J. Innate Immun.* **7**, 153–164 (2015).

Acknowledgements

We thank Dr. Qiang Ding (Tsinghua University, China) for providing SARS-CoV-2 GFP/ΔN trVLP and Caco2-N cells, Dr. Zhengfan Jiang (Peking University, China) for providing Flag-VISA-d6 mutant, and Dr. Hongbing Shu (Wuhan University, China) for providing a series of key reagents. This work was supported by grants from the National Key Research and Development Program of China (2024YFA1803100 to C.-Q. L.), the National Natural Science Foundation of China (32270757, 32070773, 32470929 to C.-Q. L.), Natural Science Foundation of Wuhan (2024040701010031 to C.-Q. L.), the State Key Laboratory for Animal Disease Control and Prevention (SKLVEB-KFKT-01K to C.-Q. L.), and the Young Top-notch Talent Cultivation Program of China and Hubei Province.

Author contributions

C.-Q.L. conceived and designed the study; M.-L.S., C.W., Z.C., H.-T.X performed the experiments; Z.C. and M.-C.L. generated and breed the mice; L.Y., J.S. and T.-N.G. performed proteomics analysis; M.-L.S., C.W., Z.C., Y.L., J.S., Y.Z., M.-C.L. and C.-Q.L. analyzed the data; C.-Q.L., M.-C.L., Y.-D.Z and Y.Z. wrote the paper.

Competing interests

The authors declare no competing interests.

Additional information

Supplementary information The online version contains supplementary material available at https://doi.org/10.1038/s41467-025-59421-x.

Correspondence and requests for materials should be addressed to Mengcheng Luo or Caoqi Lei.

Peer review information *Nature Communications* thanks Fajian Hou, and the other, anonymous, reviewer(s) for their contribution to the peer review of this work. A peer review file is available.